The onset of the Dead Sea transform based on calcite age-strain analyses

P. Nuriel[1]*, R. Weinberger[1,2], A.R.C. Kylander-Clark[3], B.R. Hacker[3], and J.P. Craddock[4].

[1]Geological Survey of Israel, 30 Malkhe Israel Street, Jerusalem 95501, Israel
[2]Department of Geological and Environmental Sciences, Ben-Gurion University, Beer-Sheva 84105, Israel
[3]Department of Earth Science, University of California, Santa Barbara, California 93106, USA
[4]Department of Geology, Macalester College, St. Paul, Minnesota 55105, USA

ABSTRACT

The onset and evolution of the Dead Sea transform are re-evaluated based on new in situ U-Pb dating and strain analyses of mechanically twinned calcites. Direct dating of 30 syn-faulting calcites from 10 different inactive fault strands of the transform indicates that the oceanic-to-continental plate boundary initiated between 20.8 and 18.5 Ma within an ~10-km-wide distributed deformation zone in southern Israel. Ages from the northern Dead Sea transform (17.1–12.7 Ma) suggest northward propagation and the establishment of a well-developed >500-km-long plate-bounding fault in 3 m.y. The dominant horizontal shortening direction recorded in the dated twinned calcites marks the onset of left-lateral motion along the evolving plate boundary. The observed changes in the strain field within individual fault strands cannot be simply explained by local "weakening effects" along strands of the Dead Sea transform or by gradual changes in the Euler pole through time.

INTRODUCTION

Direct dating of brittle fault activity and deciphering the associated stress-strain field are key factors in tectonic reconstructions and paleoseismic studies. Yet, direct ages of fault activity coupled with robust strain directions along plate-bounding faults are rare. Here we focus on the Dead Sea transform (DST)—the plate boundary that accommodates the relative motion between the Africa (Sinai) and Arabia plates—and provide new insights into the onset and evolution of this seismically active system.

A host of stratigraphic and structural evidence paints a general picture of the evolution of the DST. There has been ~105 km of left-lateral offset across the boundary (Quennell, 1958; Freund et al., 1970; Garfunkel, 1981; Joffe and Garfunkel, 1987). The onset of this motion post-dates 22–20 Ma, based on offset magmatic dikes (Eyal et al., 1981), the ages of the oldest basin-fill sediments along the transform (Garfunkel, 1981), and additional kinematic considerations related to the opening of the Red Sea (Joffe and Garfunkel, 1987). This strike-slip motion may have been preceded by normal faulting, suggesting that the present DST was localized within an old faulted terrane (Bosworth et al., 2005; Avni et al., 2012). Mesostructural analyses indicate regional NNW–SSE horizontal shortening associated with the left-lateral motion along the transform (Eyal and Reches, 1983). The trajectories of this strain field vary locally adjacent

to the transform, aligning either sub-parallel or sub-perpendicular to strands of the system (Garfunkel, 1981; Weinberger et al., 2009). This regional strain field was dominant from the Neogene to Recent. However, eastward migration of the Sinai-Arabia Euler pole through time has resulted in rearrangement of the plate boundary, causing local changes in the strain field (Gomez et al., 2007; Marco, 2007; Schattner and Weinberger, 2008; Weinberger et al., 2009).

Many aspects of the evolution of the DST are not yet understood. For example, when and where did the transform system initiate (Omar and Steckler, 1995; Wolfenden et al., 2004)? Did the transform propagate northward or southward (Ben-Avraham and Lyakhovsky, 1992; Omar and Steckler, 1995)? Was the strike-slip motion localized or distributed within a wider deformation zone (Wesnousky, 1988; Marco, 2007)? Did the system initiate by reactivation of pre-existing faults (Bosworth et al., 2005; Avni et al., 2012)? And, did the strain field fluctuate regionally through time (Eyal, 1996) or just locally adjacent to the transform (Garfunkel, 1981)? Understanding these issues of the archetypal DST may shed light on similar strike-slip boundaries elsewhere on Earth.

Here we reveal the early stages of the DST evolution by using two approaches: U-Pb calcite dating (Li et al., 2014; Coogan et al., 2016; Ring and Gerdes, 2016; Roberts and Walker, 2016) to obtain absolute time constraints on fault slip, and calcite twin analyses to decode the finite strain field related to long-term fault activity

(Burkhard, 1993). The results provide for the first time combined U-Pb ages and paleo-strain directions of individual calcite crystals from fault zones.

METHODS AND RESULTS

We studied syn-faulting calcite in two areas—Hermon in northern Israel, and Elat in southern Israel—that are ~500 km apart along the DST (Fig. 1A, inset). In each area, we sampled fault zones located away from the currently active strands of the transform that might preserve the ages and strain directions of early phases of the DST history. In the Hermon region, we sampled two localities along the ~8-km-wide shear zone in the Arabian plate which consists of northeast-southwest–striking faults and grabens (Fig. 1A). We sampled eight localities in the Elat region where the DST is associated with an ~10-km-wide shear zone in the Sinai sub-plate (Figs. 1B and 1C).

Fault-related calcite precipitates such as breccia cement, sheared fault coating, and associated microstructures were examined (Fig. 2; Fig. DR1 in the GSA Data Repository[1]) to assess the temporal relationships between deformation and calcite precipitation (Nuriel et al., 2012b). A total of 30 syntectonic calcite precipitates were dated by U-Pb laser ablation–multicollector–inductively coupled plasma–mass spectrometry (LA-MC-ICPMS). The U-Pb calcite geochronology follows standard methods described elsewhere (Li et al., 2014; Coogan et al., 2016; Ring and Gerdes, 2016; Roberts and Walker, 2016) with several lab specifications (Kylander-Clark et al., 2013) and modifications (see Fig. DR2). For mass-bias correction of the measured $^{238}U/^{206}Pb$ and $^{207}Pb/^{206}Pb$ ratios, we used the 3.001 ± 0.012 (2σ) Ma calcite speleothem ASH-15D standard
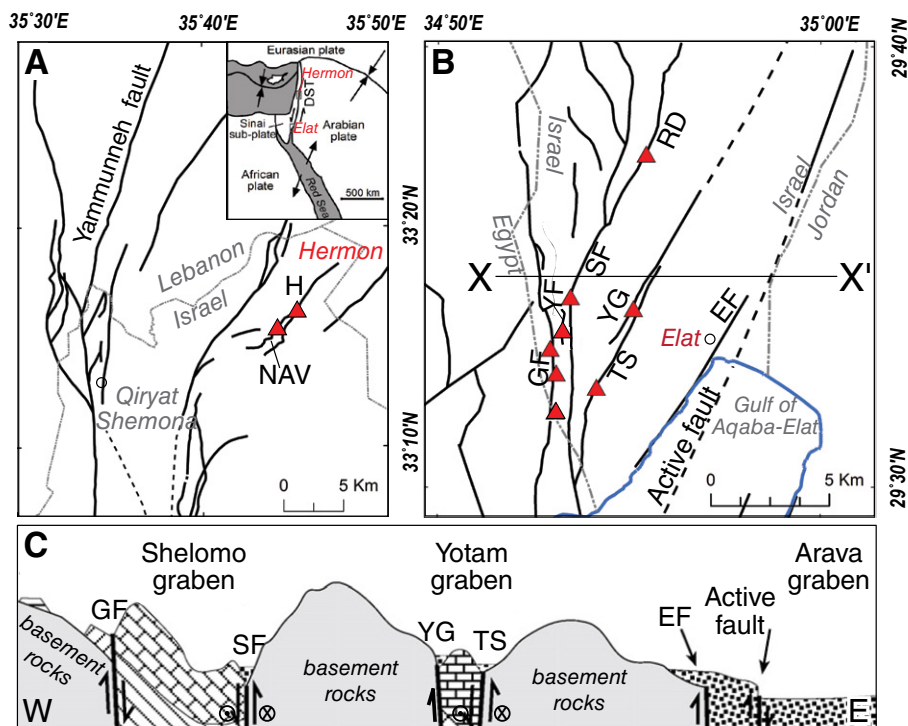
---

*E-mail: nuriel@gsi.gov.il

Figure 1. Location maps and cross-section along the Dead Sea transform (DST), Israel. Triangles mark sampling sites of fault-related calcite precipitates. A: Setting of Guvta (H) and Newe Ative graben (NAV) fault zones in the northern, Hermon region. Inset shows general plate-tectonic configuration of left-lateral Dead Sea transform (DST). B: Setting of Gishron (GF), Yehoshafat (YF), Shelomo (SF), Roded (RD), Yotam (YG), Tsefahot (TS), and Elat (EF) fault zones in southern, Elat region; solid lines mark trace of major faults at surface, and dashed lines mark inferred location of major faults in subsurface (modified after Beyth et al., 2012, and Sneh and Weinberger, 2014). C: Schematic cross-section through Elat region showing ~10-km-wide deformation zone with several major approximately north-south–striking faults that form two prominent grabens (Shelomo and Yotam) and juxtapose mainly Proterozoic crystalline basement rocks against Cambrian to Neogene sedimentary sequence (Eyal, 1973) (modified after Marco, 2007).
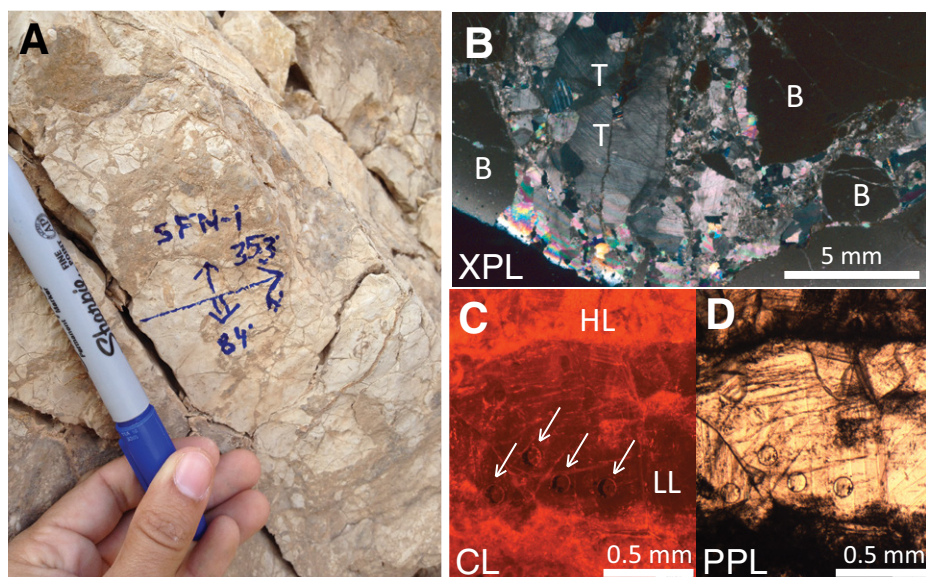

Figure 2. Example of fault-related calcite from Shelomo fault zone, Israel. A: Subvertical, approximately north-striking fault-wall breccia. B: Breccia fragments (B) and coarse-grained calcite cement, showing twins (T) under cross-polarized light (XPL). C,D: Cathodoluminescence (CL, panel C) and plane-polarized light (PPL) (panel D) images of laser ablation spot analyses (arrows) within calcite cement. Note high luminescence (HL) of host rock relative to weakly luminescent dated calcite (LL). Additional microstructure observations are given in Figure DR1 (see footnote 1).

previously dated by thermal ionization mass spectrometry (TIMS) (Mason et al., 2013; Vaks et al., 2013) and NIST-614 glass, respectively. Variation in the U-Pb ratios among individual spot analyses of single samples allows determination of a Tera-Wasserburg intercept age with 2σ errors better than 6% for most samples (see an example in Fig. 3 and in Fig. DR2). The ages of syntectonic calcite range from 21 to 6 Ma ($n = 28$; Fig. 4), and ages of 92 and 57 Ma ($n = 2$; Fig. DR2) were obtained for host-rock carbonate and an older generation of calcite veins, respectively.

Calcite twins mechanically at low differential stresses (~10 MPa) either during or shortly after calcite crystallizes in an active fault zone. While fault kinematics are susceptible to an instantaneous strain field during earthquake events (Fossen, 2010), calcite twin analyses can be used to infer the finite strain field. For calcite strain analyses, we used four-axis universal stage measurements of twin orientations and the crystallographic orientation of the host crystals to calculate the maximum shortening direction (ε_1) using a least-squares technique (Groshong et al., 1984; see more in Fig. DR3). The dominant maximum shortening ε_1 direction is horizontal, ranging from approximately NNW-SSW (11 samples) to approximately north-south (7 samples) and to approximately NNE-SSW (9 samples) directions (Fig. 4; Fig. DR3). Only two fault samples have oblique ε_1 shortening directions that are plunging 56°–51° (samples GFS1 and YG3). Host-rock carbonate with an age of 92 Ma next to the Roded fault (sample RD3a) has a subvertical ε_1 shortening direction that is plunging 68°. An older vein generation (sample NAV2Vb, 57 Ma) that is offset by DST–related structure (sample NAV3Vb) has east-west ε_1 directions. Sample TS2 is very different both in age (6 Ma) and ε_1 direction (east-west) and is therefore considered as an outlier.

DISCUSSION AND CONCLUSIONS

Combining the U-Pb ages with the shortening direction determined from calcite twins reveals a coherent picture for the onset and evolution of the DST. Left-lateral motion initiated by 20.8 ± 2.3 Ma in the southern, Elat part of the transform and reached the northern, Hermon region by 17.1 ± 0.3 Ma. These ages are compatible with northward propagation of fault activity to establish a well-developed, >500-km-long plate-bounding fault in 3 m.y., and provide further support to studies that show a northward progression of slip from the Gulf of Aqaba-Elat (Bar et al., 1974). These ages also support the chronological framework of the DST inferred by indirect methods (Eyal et al., 1981; Garfunkel, 1981) and exclude the possibility that the transform boundary initiated later at ca. 14 Ma (Bosworth et al., 2005). In the Elat shear zone, the oldest ages—20.8, 20.1, 19.0, 18.6, and 18.5 Ma—are from the westernmost and easternmost bounding faults (Gishron and Tsefahot fault

zones; Fig. 1C), and these faults have maximum horizontal shortening directions that are compatible with left-lateral motion. Hence, the Elat region preserves a record of the oldest known part of the DST system so far. The results further reveal that the transform initiated within an ~10-km-wide distributed deformation zone (from the Gishron to the Tsefahot faults; Fig. 1C). The cessation of fault activity in the Elat shear zone at 12.7 Ma was followed by the formation of a flat erosion surface that truncates the structures (Fig. 1C).

The results do not support reactivation of preexisting normal faults, because calcite twins with subvertical maximum shortening directions are absent (see Fig. DR3). The dominant maximum horizontal shortening directions fluctuated between NNW-SSE and NNE-SSW during the period from 20.8 to 12.7 Ma. Such fluctuations in the strain field within individual segments cannot be simply explained by local "weakening effects" along fault strands of the DST (Garfunkel, 1981) or by gradual migration of the Euler pole through time (Gomez et al., 2007; Marco, 2007; Weinberger et al., 2009).

REFERENCES CITED

Avni, Y., Segev, A., and Ginat, H., 2012, Oligocene regional denudation of the northern Afar dome: Pre- and syn-breakup stages of the Afro-Arabian plate: Geological Society of America Bulletin, v. 124, p. 1871–1897, doi:10.1130/B30634.1.

Bar, M., Kolodny, Y., and Bentor, Y.K., 1974, Dating faults by fission track dating of epidotes—An attempt: Earth and Planetary Science Letters, v. 22, p. 157–162, doi:10.1016/0012-821X(74)90076-4.

Ben-Avraham, Z., and Lyakhovsky, V., 1992, Faulting processes along the northern Dead Sea transform and the Levant margin: Geology, v. 20, p. 1139–1142, doi:10.1130/0091-7613(1992)020<1139: FPATND>2.3.CO;2.

Beyth, M., Eyal, Y., and Garfunkel, Z., 2012, Geological map of Israel, sheet 26-I, II: Elat: Jerusalem, Israel Geological Survey, scale 1:50,000.

Bosworth, W., Huchon, P., and McClay, K., 2005, The Red Sea and Gulf of Aden Basins: Journal of African Earth Sciences, v. 43, p. 334–378, doi: 10.1016/j.jafrearsci.2005.07.020.

Burkhard, M., 1993, Calcite twins, their geometry, appearance and significance as stress-strain markers and indicators of tectonic regime: A review: Journal of Structural Geology, v. 15, p. 351–368, doi:10.1016/0191-8141(93)90132-T.

Coogan, L.A., Parrish, R.R., and Roberts, N.M., 2016, Early hydrothermal carbon uptake by the upper oceanic crust: Insight from in situ U-Pb dating: Geology, v. 44, p. 147–150, doi:10.1130/G37212.1.

Eyal, M., Eyal, Y., Bartov, Y., and Steinitz, G., 1981, The tectonic development of the western margin of the Gulf of Elat (Aqaba) rift: Tectonophysics,

v. 80, p. 39–66, doi:10.1016/0040-1951(81) 90141-4.

Eyal, Y., 1973, The tectonics of the Shelomo and Yotam grabens, Elat, Israel: Israel Journal of Earth Sciences, v. 22, p. 165–184.

Eyal, Y., 1996, Stress field fluctuations along the Dead Sea rift since the middle Miocene: Tectonics, v. 15, p. 157–170, doi:10.1029/95TC02619.

Eyal, Y., and Reches, Z., 1983, Tectonic analysis of the Dead Sea Rift Region since the Late-Cretaceous
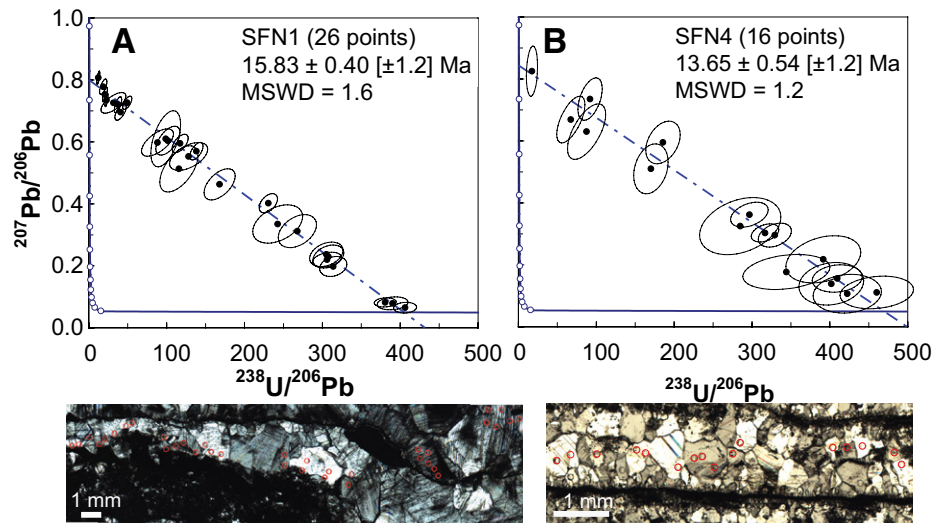
Figure 3. U-Pb Tera-Wasserburg concordia plots for samples SFN1 and SFN4 from Shelomo fault zone, Israel. Locations of laser ablation spot analyses (red circles) are indicated on cross-polarized microscopy images. Additional Tera-Wasserburg plots are given in Figure DR2 (see footnote 1). MSWD—mean square of weighted deviates.
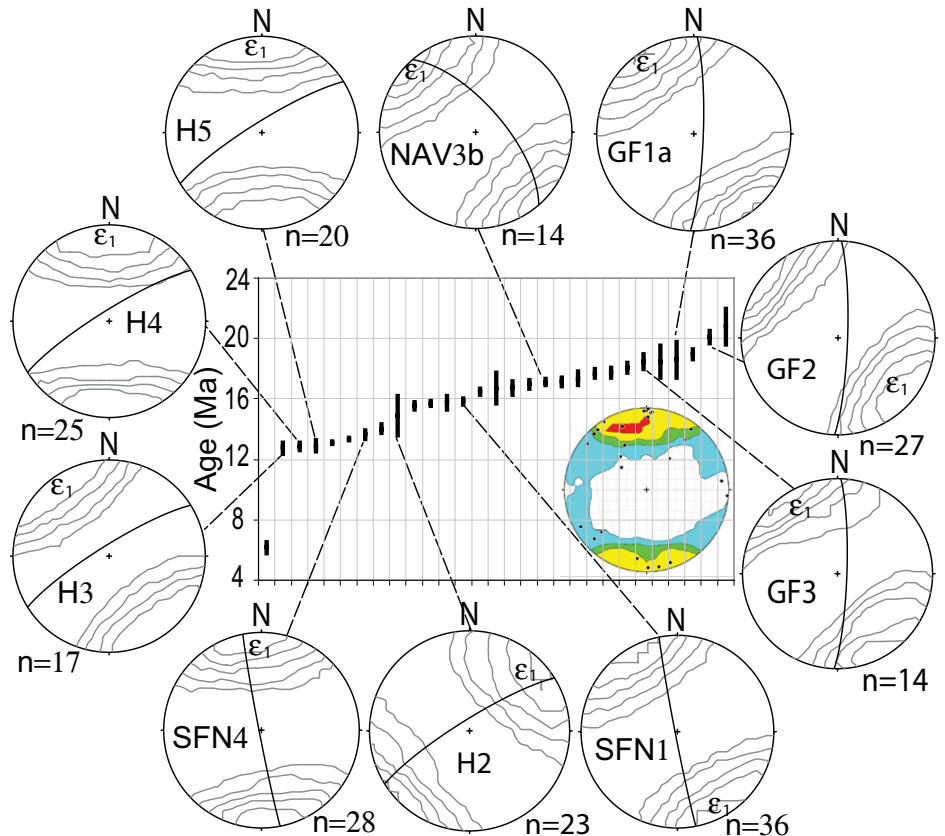

Figure 4. Summary of U-Pb ages and calcite-twin strain analyses of fault-related calcite from Dead Sea transform (DST), Israel. Box heights represent 2σ errors. Lower-hemisphere stereoplots include contours of maximum shortening strain axis (ε_1). Great circles represent fault orientations. Colored inset shows contours of all ε_1 with dominant NNW-SSE direction for all strain analyses (n = 28). Additional stereoplots are given in Figure DR3 (see footnote 1).

based on mesostructures: Tectonics, v. 2, p. 167–185, doi:10.1029/TC002i002p00167.

Fossen, H., 2010, Structural Geology: Cambridge, UK, Cambridge University Press, 463 p., doi:10.1017/CBO9780511777806.

Freund, R., Garfunkel, Z., Zak, I., Goldberg, M., Weissbrod, T., and Derin, B., 1970, The shear along the Dead Sea rift: Philosophical Transactions of the Royal Society of London A, v. 267, p. 107–130, doi:10.1098/rsta.1970.0027.

Garfunkel, Z., 1981, Internal structure of the Dead Sea leaky transform (rift) in relation to plate kinematics: Tectonophysics, v. 80, p. 81–108, doi:10.1016/0040-1951(81)90143-8.

Gomez, F., Nemer, T., Tabet, C., Khawlie, M., Meghraoui, M., and Barazangi, M., 2007, Strain partitioning of active transpression within the Lebanese restraining bend of the Dead Sea Fault (Lebanon and SW Syria), in Cunningham, W.D., and Mann, P., eds., Tectonics of Strike-Slip Restraining and Releasing Bends: Geological Society of London Special Publication 290, p. 285–303, doi:10.1144/290.10.

Groshong, R.H.J., Teufel, L.W., and Gasteiger, C.M., 1984, Precision and accuracy of the calcite strain-gage technique: Geological Society of America Bulletin, v. 95, p. 357–363, doi:10.1130/0016-7606(1984)95<357:PAAOTC>2.0.CO;2.

Joffe, S., and Garfunkel, Z., 1987, Plate kinematics of the circum Red Sea—A re-evaluation: Tectonophysics, v. 141, p. 5–22, doi:10.1016/0040-1951(87)90171-5.

Kylander-Clark, A.R.C., Hacker, B.R., and Cottle, J.M., 2013, Laser-ablation split-stream ICP petrochronology: Chemical Geology, v. 345, p. 99–112, doi:10.1016/j.chemgeo.2013.02.019.

Li, Q., Parrish, R., Horstwood, M., and McArthur, J., 2014, U-Pb dating of cements in Mesozoic ammonites: Chemical Geology, v. 376, p. 76–83, doi:10.1016/j.chemgeo.2014.03.020.

Marco, S., 2007, Temporal variation in the geometry of a strike-slip fault zone: Examples from the Dead Sea Transform: Tectonophysics, v. 445, p. 186–199, doi:10.1016/j.tecto.2007.08.014.

Mason, A.J., Henderson, G.M., and Vaks, A., 2013, An acetic acid–based extraction protocol for the recovery of U, Th and Pb from calcium carbonates for U-(Th)-Pb geochronology: Geostandards and Geoanalytical Research, v. 37, p. 261–275, doi:10.1111/j.1751-908X.2013.00219.x.

Nuriel, P., Rosenbaum, G., Zhao, J.-X., Feng, Y., Golding, S.D., Villemant, B., and Weinberger, R., 2012b, U-Th dating of striated fault planes: Geology, v. 40, p. 647–650, doi:10.1130/G32970.1.

Omar, G.I., and Steckler, M.S., 1995, Fission track evidence on the initial rifting of the Red Sea: Two pulses, no propagation: Science, v. 270, p. 1341, doi:10.1126/science.270.5240.1341.

Quennell, A.M., 1958, The structural and geomorphologic evolution of the Dead Sea Rift: Journal of the Geological Society, v. 114, p. 1–24, doi:10.1144/gsjgs.114.1.0001.

Ring, U., and Gerdes, A., 2016, Kinematics of the Alpenrhein-Bodensee graben system in the Central Alps: Oligocene/Miocene transtension due to formation of the Western Alps arc: Tectonics, v. 35, p. 1367–1391, doi:10.1002/2015TC004085.

Roberts, N.M., and Walker, R.J., 2016, U-Pb geochronology of calcite-mineralized faults: Absolute timing of rift-related fault events on the northeast Atlantic margin: Geology, v. 44, p. 531–534, doi:10.1130/G37868.1.

Schattner, U., and Weinberger, R., 2008, A mid-Pleistocene deformation transition in the Hula basin, northern Israel: Implications for the tectonic evolution of the Dead Sea Fault: Geochemistry Geophysics Geosystems, v. 9, Q07009, doi:10.1029/2007GC001937.

Sneh, A., and Weinberger, R., 2014, Major structures of Israel and environs: Jerusalem, Geological Survey of Israel, scale 1:500,000.

Vaks, A., Woodhead, J., Bar-Matthews, M., Ayalon, A., Cliff, R.A., Zilberman, T., Matthews, A., and Frumkin, A., 2013, Pliocene–Pleistocene climate of the northern margin of Saharan–Arabian Desert recorded in speleothems from the Negev Desert, Israel: Earth and Planetary Science Letters, v. 368, p. 88–100, doi:10.1016/j.epsl.2013.02.027.

Weinberger, R., Gross, M. R., and Sneh, A., 2009, Evolving deformation along a transform plate boundary: Example from the Dead Sea Fault in northern Israel: Tectonics, v. 28, TC5005, doi:10.1029/2008TC002316.

Wesnousky, S., 1988, Seismological and structural evolution of strike-slip faults: Nature, v. 335, p. 340–343, doi:10.1038/335340a0.

Wolfenden, E., Ebinger, C., Yirgu, G., Deino, A., and Ayalew, D., 2004, Evolution of the northern Main Ethiopian rift: Birth of a triple junction: Earth and Planetary Science Letters, v. 224, p. 213–228, doi:10.1016/j.epsl.2004.04.022.